INTERNATIONAL JOURNAL FOR NUMERICAL METHODS IN FLUIDS
Int. J. Numer. Meth. Fluids 2003; **42**:89–116 (DOI: 10.1002/fld.492)

A new hybrid turbulence modelling strategy for industrial CFD

B. Basara[1,*,†] and S. Jakirlic[2]

[1] *AVL List GmbH, Advanced Simulation Technologies, Hans List Platz 1, A-8020 Graz, Austria*
[2] *Chair of Fluid Mechanics and Aerodynamics, Darmstadt University of Technology, Petersenstrasse 30, 64287 Darmstadt, Germany*

SUMMARY

This paper presents a new strategy for turbulence model employment with emphasis on the model's applicability for industrial computational fluid dynamics (CFD). In the hybrid modelling strategy proposed here, the Reynolds stress and mean rate of strain tensors are coupled via Boussinesq's formula as in the standard k–ε model. However, the turbulent kinetic energy is calculated as the sum of the normal Reynolds-stress components, representing the solutions of the appropriate transport equations. The equations governing the Reynolds-stress tensor and dissipation rate have been solved in the framework of a 'background' second-moment closure model. Furthermore, the structure parameter C_μ has been re-calculated from a newly proposed functional dependency $f(\overline{u_i u_j}, \partial U_i/\partial x_j)$ rather than kept constant. This new definition of C_μ has been assessed by using direct numerical simulation (DNS) results of several generic flow configurations featuring different phenomena such as separation, reattachment and rotation. Comparisons show a large departure of C_μ from the commonly used value of 0.09. The model proposed is computationally validated in a number of well-proven fluid flow benchmarks, e.g. backward-facing step, 180° turn-around duct, rotating pipe, impinging jet and three-dimensional (3D) Ahmed body. The obtained results confirm that the present hybrid model delivers a robust solution procedure while preserving most of the physical advantages of the Reynolds-stress model over simple k–ε models. A low Reynolds number version of the hybrid model is also proposed and discussed. Copyright © 2003 John Wiley & Sons, Ltd.

KEY WORDS: Reynolds-averaged Navier–Stokes equations; hybrid turbulence model; finite volume method; low-*Re* number model

1. INTRODUCTION

The progress of turbulence models based on Reynolds-averaged Navier–Stokes (RANS) equations has been somewhat stagnant in recent years and to date, there is no turbulence model which can be considered 'universal' and which achieves acceptable accuracy in all flows of practical interest [1]. Alternative approaches, e.g. large eddy simulation (LES) or direct

* Correspondence to: B. Basara, AVL List GmbH, Hans-List-Platz 1, A-8020 Graz, Austria.
† E-mail: branislav.basara@avl.com

Received 26 May 2002
Revised 6 January 2003

numerical simulations (DNS) are too costly for most engineering calculations and require additional modelling solutions for other flow classes e.g. multiphase flow, combustion, etc., which still have to be resolved. As an outcome, the RANS framework, in conjunction with statistical turbulence models, can be expected to remain the main 'tool' to solve practical industrial applications for a long time. A large number of turbulence models exists, varying from very simple to very complex forms, and although the majority of them have been tested on the same standard benchmarks, there is no consensus about which model is best suited for which application. However, it is generally accepted that the Reynolds–stress model (RSM) is the best RANS model for the description of turbulence.

The RSM solves transport equations for the Reynolds stresses, each equation comprising terms describing the rate of change, convection, production, diffusion, redistribution and dissipation. The latest three terms require modelling. Although one can argue about some modelling issues, the accuracy of the RSM in capturing flow physics has nevertheless been shown to be superior over other models when computing the flow configurations of practical relevance (e.g. References [2–4]). On the other hand, there are numerical aspects of this model that prevent its use for a wide range of industrial flows. The main 'numerical' obstacle is the coupling between velocity, pressure and Reynolds stresses in the momentum equations, although some methods for 'coupling' improvements have been developed to date. It must also be kept in mind that industrial computational fluid dynamics (CFD) users aim at reducing the meshing time by using different 'automatic' grid generators, which regularly create unstructured grids, very often with poor quality and even consisting of arbitrary shaped cells. Such grids with computationally awkward cells lead to increased problems regarding 'coupling' and generally to a decrease of the convergence rate. Keeping in mind some additional uncertainties arising from the definition of boundary conditions for industrial applications and the geometrical complexity of flow configurations that often include moving parts, it is inevitable that industrial CFD users require less complicated and more robust turbulence model.

One solution is the eddy–viscosity turbulence model. In this model group, the turbulent stresses are proportional to the mean rate of strain [5]. Even in its simplest forms as a 'zero-equation' model (based on the Prandtl's mixing length hypothesis, e.g. Reference [6]) or a 'one-equation' model (based on the transport equation either for the kinetic energy of turbulence, e.g. Reference [7], or for the turbulent viscosity ν_t, e.g. Reference [8]), this modelling concept is very often used for industrial flows, e.g. in the aerospace industry, for turbomachinery etc. As these models usually require a length scale to be prescribed (corresponding either to the flow dimensions or to the wall distance), they are limited to the narrow range of the thin shear layer flows. It must be admitted however, that the limit of the models' applicability could be extended by modifying appropriately the model equations (see e.g. Reference [9]). Better accuracy and universality has been achieved with two-equation eddy–viscosity models. Among many models of this type, the k–ε model is the most popular. The Boussinesq's ansatz is in many occasions blamed for the poor performance of the model. The implicit isotropic assumption of such formulations, where eddy viscosity is introduced as a scalar, is an additional cause of inaccuracy. Moreover, constants are deduced from measurements by assuming local equilibrium and taken as a fixed value for the entire flow field. In the standard k–ε model, the structure parameter C_μ is taken to be equal to 0.09. Regardless of these irregularities, the k–ε model is certainly the most widely used model for engineering computations. Contrary to the RSM, its implementation is numerically robust due to the

simplicity of the model and at the same time providing an acceptable level of accuracy for some applications.

An alternative approach is proposed in this paper. The aim is to offer a less 'troublesome' use of at least parts of the RSM by achieving a compromise between robustness, speed and accuracy. Concerning the accuracy, it seems that the use of Reynolds-stress equations to calculate turbulent kinetic energy is unavoidable; hence, this is the basis of the modelling approach proposed here. Calculated Reynolds stresses are used to update the turbulence viscosity, which is then used in the momentum equations via the eddy–viscosity relationship. The dissipation rate equation is also solved in the form commonly used in the framework of the Reynolds-stress closures. It could be expected that such a combined model is more accurate than the standard k–ε model and more robust than the full RSM. A remaining possibility regarding the eddy viscosity approach is to correct the constant C_μ by using available Reynolds stresses. To analyse the behaviour of C_μ, a DNS database was used for several generic flows, such as fully developed flows in a plane channel [10], the axially rotating pipe [11] and the flow over a backward facing step [12]. By using DNS data, the structure parameter being the ratio of shear stresses and turbulent kinetic energy is recalculated showing a departure from a constant value. Furthermore, a new invariant formulation for C_μ is proposed, based on the application of least squares approach on the Boussinesq correlation.

A number of cases predicted with the 'hybrid turbulence model' are presented in this paper. These results show that such a modelling approach can be an alternative solution to existing turbulence models. It is important to point out that the proposed model differs from the usually proposed zonal models, which suffer from numerical instability due to the interface between different models employed in the same calculation domain.

2. MATHEMATICAL MODEL

The mathematical model is based on the RANS equations. The momentum equations, given in Cartesian tensor notation, are

$$\rho \frac{DU_i}{Dt} = -\frac{\partial P}{\partial x_i} + \frac{\partial}{\partial x_j}\left[\mu\left(\frac{\partial U_i}{\partial x_j} + \frac{\partial U_j}{\partial x_i} - \frac{2}{3}\frac{\partial U_k}{\partial x_k}\delta_{ij}\right) - \rho\overline{u_i u_j}\right] \tag{1}$$

where U_i stands for the mean velocity vector, P is the static pressure and ρ and μ are the fluid density and the dynamic viscosity, respectively. The correlations $\overline{u_i u_j}$, known as the Reynolds stresses, are additional unknowns in this set of equations, which leave the number of unknowns larger then the number of equations.

In the k–ε eddy–viscosity model, the Reynolds stresses are evaluated from Bousinessq's assumption, given by

$$-\rho\overline{u_i u_j} = 2\mu_t S_{ij} - \tfrac{2}{3}\rho\delta_{ij}k \tag{2}$$

where S_{ij} is the mean rate of strain tensor, given as $S_{ij} = \frac{1}{2}(\partial U_i/\partial x_j + \partial U_j/\partial x_i)$ and the turbulence viscosity μ_t is evaluated from

$$\mu_t = C_\mu \rho \frac{k^2}{\varepsilon} \tag{3}$$

In order to close the k–ε model, it is necessary to solve equations for the turbulent kinetic energy, k, and its dissipation rate, ε:

$$\rho \frac{Dk}{Dt} = \rho(P_k - \varepsilon) + \frac{\partial}{\partial x_j}\left[\left(\mu + \frac{\mu_t}{\sigma_k}\right)\frac{\partial k}{\partial x_j}\right] \tag{4}$$

$$\rho \frac{D\varepsilon}{Dt} = \rho\left(C_{\varepsilon 1}P_k + C_{\varepsilon 3}k\frac{\partial U_k}{\partial x_k} - C_{\varepsilon 2}\varepsilon\right)\frac{\varepsilon}{k} + \frac{\partial}{\partial x_j}\left[\left(\mu + \frac{\mu_t}{\sigma_\varepsilon}\right)\frac{\partial \varepsilon}{\partial x_j}\right] \tag{5}$$

where the production of turbulent kinetic energy is given by $P_k = -\overline{u_i u_j}\partial U_i/\partial x_j$. The model coefficients appearing in the above equations are assigned their standard values [13]:

$$C_\mu = 0.09, \quad C_{\varepsilon 1} = 1.44, \quad C_{\varepsilon 2} = 1.92, \quad \sigma_k = 1.0, \quad \sigma_\varepsilon = 1.3$$

In the case of the second moment turbulence closure, the Reynolds stresses are obtained from the solution of the differential transport equation:

$$\frac{\partial \overline{u_i u_j}}{\partial t} + U_k\frac{\partial \overline{u_i u_j}}{\partial x_k} = -\left(\overline{u_i u_k}\frac{\partial U_j}{\partial x_k} + \overline{u_j u_k}\frac{\partial U_i}{\partial x_k}\right) + \frac{\partial}{\partial x_k}\left[\nu\frac{\partial \overline{u_i u_j}}{\partial x_k} + C_s\frac{k}{\varepsilon}\overline{u_k u_l}\frac{\partial \overline{u_i u_j}}{\partial x_l}\right] - \frac{2}{3}\delta_{ij}\varepsilon + \Phi_{ij} \tag{6}$$

In this equation, the diffusion by turbulence fluctuations was modelled with a simple gradient-transport hypothesis ($C_s = 0.22$) and viscous dissipation was assumed to be isotropic. The ability to abandon the wall topography parameters and a local distance from a solid wall from the second-moment closure has been viewed as an important prerequisite for wider applications in geometrically complex flows. Dependency of the results due to different numerical interpretation of terms acting normal to the wall has to be avoided. The model proposed by Speziale *et al.* [14] showed that the inclusion of second-order, non-linear terms in the model of the pressure–strain term can serve, at least in part, as a substitute for a wall-distance–dependent pressure–reflection term in the model of Gibson and Launder [15]. This model also shows an improvement in reproducing the turbulence interaction in stagnation regions. Thus the complete pressure–strain term is of the form:

$$\phi_{ij} = -(C_1\varepsilon + C_1^* P_k)b_{ij} + C_2\varepsilon\left(b_{ik}b_{jk} - \frac{1}{3}b_{mn}b_{mn}\delta_{ij}\right) + [C_3 - C_3^*(b_{mn}b_{mn})^{1/2}]kS_{ij} + C_4 k\left(b_{ik}S_{jk} + b_{jk}S_{ik} - \frac{2}{3}b_{mn}S_{mn}\delta_{ij}\right) + C_5 k(b_{ik}W_{jk} + b_{jk}W_{ik}) \tag{7}$$

where $b_{ij} = \overline{u_i u_j}/(2k) - \delta_{ij}/3$ and $W_{ij} = 0.5(\partial U_i/\partial x_j - \partial U_j/\partial x_i)$ are the Reynolds-stress anisotropy and the mean vorticity tensors, respectively. The dissipation rate was obtained from the standard equation

$$\frac{D\varepsilon}{Dt} = \left(C_{\varepsilon 1}P_k + C_{\varepsilon 3}k\frac{\partial U_k}{\partial x_k} - C_{\varepsilon 2}\varepsilon\right)\frac{\varepsilon}{k} + \frac{\partial}{\partial x_j}\left(C_\varepsilon\frac{k}{\varepsilon}\overline{u_i u_j}\frac{\partial \varepsilon}{\partial x_i}\right) \tag{8}$$

The turbulent kinetic energy, k, is obtained from the sum of the normal Reynolds stresses. The coefficients in Equations (7) and (8) are those assigned by the model's originators (see original reference [14]).

In the present study, all models have been used in conjunction with standard wall functions (apart from Chapter 6, dealing with the near-wall variant of the hybrid model). The standard wall function is applied by introducing wall turbulent viscosity, thus

$$\mu_{\mathrm{w}} = \frac{y_P^+}{U_P^+}\,\mu \tag{9}$$

where

$$U_P^+ = \begin{cases} y_P^+ & \text{if } y_P^+ < 11.63 \\ \dfrac{1}{\kappa}\ln(E y_P^+) & \text{if } y_P^+ \geqslant 11.63 \end{cases} \tag{10}$$

The non-dimensional wall distance is given as

$$y^+ = \frac{\rho C_\mu^{1/4} k^{1/2} \delta n}{\mu} \tag{11}$$

where δn denotes the normal distance from the near-wall node to the wall. The flux of turbulent kinetic energy at the wall is taken to be zero, a condition simply enforced by setting the appropriate finite-difference coefficients to zero. The values of k at the node closest to the wall is therefore obtained from the solution of its equation there. A single modification to the standard equation is required: it concerns the way in which the rate of production of k is evaluated at the grid nodes closest to the wall. Dissipation rate ε is fixed for the first-to-wall cells by assuming that turbulence is in local equilibrium. In the case of Reynolds stresses there are two main approaches, the first one was proposed by Lien and Leschziner [16] who derived the Reynolds stresses in the first-to-wall cell by focussing on the stress equation (6) applicable to the local energy equilibrium. The 'log-law' derived stresses are wall oriented and should be transformed to the Cartesian co-ordinate system to be in agreement with the procedure needed for non-orthogonal geometry. The second approach in which the Reynolds-stress components are solved at the nodes closest to the wall seems to be more robust, but is tricky to implement with wall functions. In this approach, the velocity gradients of mean velocity that enter into the various production rate terms are evaluated from differentiation of the log-law (see Chapter 4).

3. HYBRID TURBULENCE MODEL (HTM): RATIONALE

An expression (3) for the turbulence viscosity can be reformulated as

$$\mu_{\mathrm{t}} = \rho C_\mu \left(\frac{k^{3/2}}{\varepsilon}\right) k^{1/2} = \rho C_\mu L_0 v_0 \tag{12}$$

where L_0 and v_0 denote characteristic length and velocity scales of turbulence, respectively. In the k–ε modelling concept these scales are provided by solving the transport equation for the turbulent kinetic energy and its dissipation rate. The C_μ coefficient is derived in the

framework of a one-equation model using the Prandtl–Kolmogoroff expression $\nu_t = C_\mu k^{1/2} L$ (see e.g. Reference [17]) and assuming local equilibrium: equality of the production and dissipation rate of the kinetic energy of turbulence and a constant shear stress $\rho\overline{uv}$ across the logarithmic law region of a turbulent boundary layer. This derivation yields the expression $C_\mu = (-\overline{uv}/k)^2$, known as the structure parameter of turbulence. Some early measurements of the boundary layer flows, such as those from Schubauer (1954, see e.g. Reference [18, p. 492]), indicated a fairly constant value of this ratio ($-\overline{uv}/k \approx 0.3$) in a large portion of the cross-section. It led to the most commonly used constant value for C_μ of 0.09. This is surely a weak point of such a model formulation, because the parameter C_μ varies not only from one flow to another but also across the same flow. Pope [19] discussed the necessity to express this coefficient as a non-trivial function of some flow parameter, e.g. S_{ij} and W_{ij}. Some authors proposed alternative values depending on the flow type, as e.g. Reference [20], who even derived a different C_μ for the channel flow depending on the bulk Reynolds number. This evaluation of C_μ indicates a range between 0.06 and 0.12 for some simpler types of flows. Rodi [21] correlated the experimental data of weak shear flows (far-field jets and wakes), where the production and dissipation rates of k differ significantly. He proposed C_μ to be a function of the average value of the ratio P_k/ε across the layer. This function is valid only for thin shear layers and imposes a range of C_μ as large as 0.03–0.6. None of these values seems to be appropriate if considering more complex flows, introducing large uncertainties in the calculations. Pourahmadi and Humphrey [22] tried to overcome this deficiency by replacing the constant value with an expression derived from the algebraic stress model for the Reynolds stresses. Predicted Reynolds stresses were equalized with Boussinesq's assumption, finally providing a value for C_μ. The results were only partly satisfactory, since the proposed formulation produced unrealistic values over a large part of the flow. Furthermore, due to its complexity, the model has not been widely used in practice. Barakos and Drikakis [23] pointed out the decisive importance of a variable C_μ for the calculations of the transonic buffet flows around airfoils.

In this work, we used DNS data to recalculate the parameter $C_\mu = (-\overline{uv}/k)^2$ for the fully developed channel flow for different bulk Reynolds numbers [10] and for the flow over a backward facing step ($Re = 5000$, Reference [12]) i.e. the parameter $C_\mu = (\sqrt{\overline{uv}^2 + \overline{uw}^2 + \overline{vw}^2}/k)^2$ for the flow in an axially rotating pipe for different rotation rates N, (symbols in Figures 1 and 2)[‡]. The C_μ profiles in the channel flow are not shown here, because they correspond closely to the non-rotating pipe ($N = 0$), Figure 2. The structure parameter approaches roughly the value 0.09 in flows, where equilibrium conditions can be expected, as e.g. in the non-rotating pipe. However, in the near-wall regions, within the separation bubble, reattaching and recovery regions as well as in rotating pipes, the deviation from the equilibrium value 0.09 is large. Of particular mention is the very low C_μ value in the axially rotating pipe flow, becoming even lower with increasing rotational intensity. This low value will be shown to be of crucial importance in capturing the flow phenomena in rotating flows (see Chapter 5). With the aim at deriving a functional dependency for C_μ, accounting for the behaviour seen in Figures 1 and 2, the following procedure is proposed.

[‡]The lines shown in Figures 1 and 2 represent the C_μ profiles obtained by applying expression (14), see discussion in the reminder of this chapter.

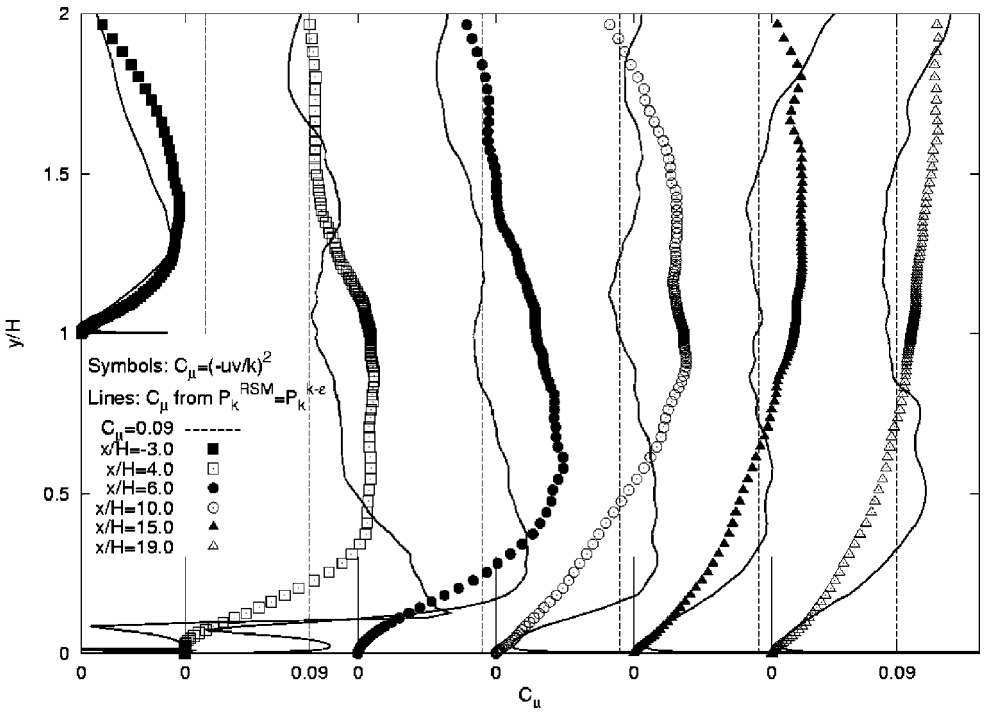

Figure 1. Profiles of the structure parameter C_μ deduced from the DNS database of the flow over a backward-facing step [12]. Lines: C_μ from the least-square approach, Equation (14). Symbols: $C_\mu = (-\overline{uv}/k)^2$.

The approach given above is extended by using Boussineq's eddy viscosity formula and the local equilibrium assumption:

$$C_\mu = \frac{(\overline{uv})^2 + (\overline{uw})^2 + (\overline{vw})^2}{k^2}\left(1 + \frac{P_{\text{irrot}}}{P_{\text{rot}}}\right) \tag{13}$$

where P_{irrot} and P_{rot} are the stress production rates being related to the normal (diagonal) components (*irrotational* part) and the shear (off diagonal) components (*rotational* part) of the Reynolds-stress tensor given as

$$P_{\text{irrot}} = \overline{u^2}\frac{\partial U}{\partial x} + \overline{v^2}\frac{\partial V}{\partial y} + \overline{w^2}\frac{\partial W}{\partial z} \quad \text{and}$$

$$P_{\text{rot}} = \overline{uv}\left(\frac{\partial U}{\partial y} + \frac{\partial V}{\partial x}\right) + \overline{uw}\left(\frac{\partial U}{\partial z} + \frac{\partial W}{\partial x}\right) + \overline{vw}\left(\frac{\partial W}{\partial y} + \frac{\partial V}{\partial z}\right)$$

respectively. Although expression (13) can satisfy some flow situations, e.g. non-separating flow in a straight channel, it cannot be used as a general formulation for complex three-dimensional cases due to its co-ordinate non-invariant form. Other similar derivations can be obtained by introducing all stress components, but usually they are characterized by a number

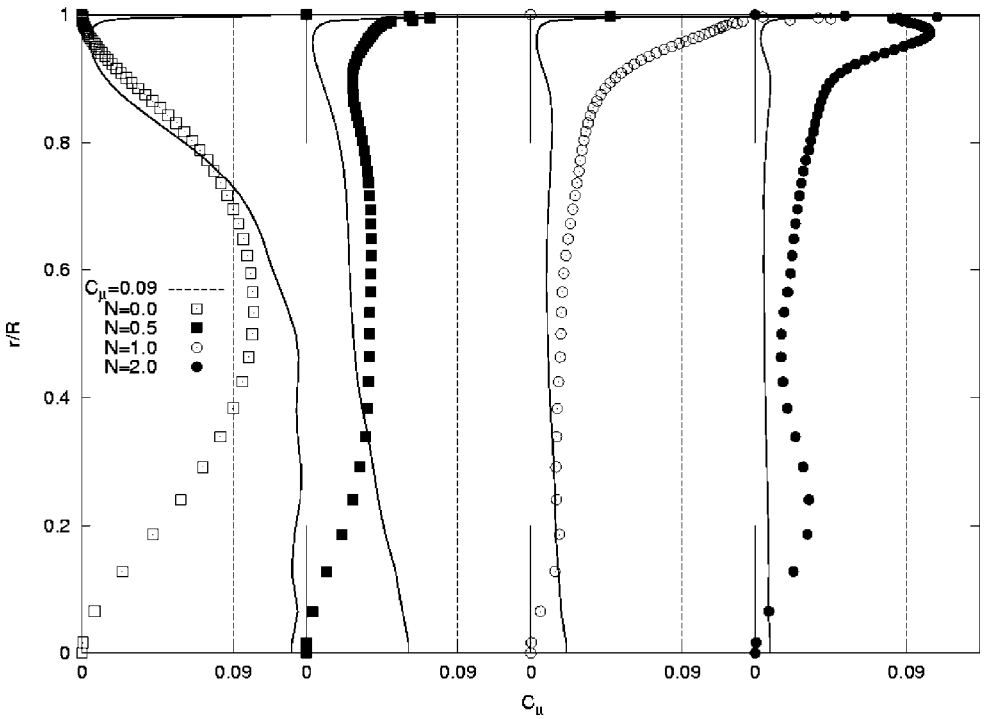

Figure 2. Profiles of the structure parameter C_μ deduced from the DNS database of the fully developed flow in an axially rotating pipe [11]. Lines: C_μ from the least-square approach, Equation (14). Symbols: $C_\mu = (\sqrt{\overline{uv}^2 + \overline{uw}^2 + \overline{vw}^2}/k)^2$.

of singularities and are very difficult to treat numerically. More complex formulations can be achieved by looking at the local co-ordinate system defined by the streamlines (tangential and normal components) but making the model too complex and departing from the basic idea to introduce a simple and robust model.

A further approach equalizes the production of turbulent kinetic energy predicted by the RSM with the production obtained by the k–ε model, thus

$$C_\mu = \left(-\overline{u_i u_j}\,\frac{\partial U_i}{\partial x_j}\right) \Big/ \left(\frac{k^2}{\varepsilon}\,S^2\right), \quad S = \sqrt{2S_{ij}S_{ij}} \tag{14}$$

This relation can be fulfilled by minimizing the error

$$E = \left(2C_\mu \frac{k^2}{\varepsilon}\,S_{ij} + \overline{u_i u_j}\right)^2 \tag{15}$$

by choice of C_μ [24]. The first derivative of (15) with C_μ is given by

$$\frac{\partial E}{\partial C_\mu} = 4\left(2C_\mu \frac{k^2}{\varepsilon}\,S_{ij} + \overline{u_i u_j}\right)\frac{k^2}{\varepsilon}\,S_{ij} \tag{16}$$

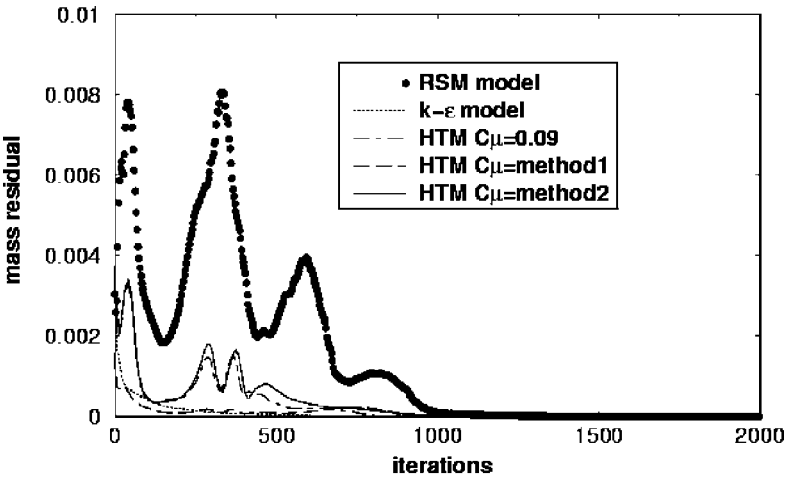

Figure 3. Convergence rate history by computation of the backward-facing flow case by all model schemes investigated.

Upon setting $\partial E/\partial C_\mu = 0$, C_μ is evaluated from

$$2C_\mu \frac{k^2}{\varepsilon} S_{ij}S_{ij} = -\overline{u_i u_j}S_{ij} \tag{17}$$

which is equivalent to Equation (14). Clearly this represents a minimum of E, since it is easily shown that

$$\frac{\partial^2 E}{\partial C_\mu^2} = 8\left(\frac{k^2}{\varepsilon}\right)^2 S_{ij}S_{ij} > 0 \tag{18}$$

The profiles of the coefficient C_μ obtained by applying expression (14), i.e. (17) (DNS data for all input variables $\overline{u_i u_j}, k, \varepsilon$ and S_{ij} were used) are compared with the structure parameter C_μ, which was mentioned earlier in this chapter, in Figures 1 and 2. This comparison reveals a similar tendency and profile shapes. Both sets of coefficients reach a level, which corresponds closely to the equilibrium value of 0.09, in a large portion of the flow behind a backward-facing step, but outside the wall region (Figure 1). Good agreement is found also in the axially rotating pipe flow, where the C_μ profiles obtained by applying the model formulation (Equation (14)) follow very low values (between 0.01 and 0.04) of the structure parameter.

The hybrid turbulence model proposed here involves the solution of the momentum equations (1) and the derived quantities in Equations (2), (3) and (14) together with the set of equations governing the Reynolds stress tensor and dissipation rate, Equations (6) and (8). In general, the model is not simple, but its use is greatly simplified with the numerical procedure given below, resulting in an overall enhancement of robustness and a decrease of computing time when compared to the RSM calculations. Figure 3 shows the mass residuals when the k–ε, RSM and HTM models are applied on the simple Cartesian orthogonal grid employed for the backward-facing step. The convergence rate of different models varies largely, but the

HTM model behaviour lies much closer to that of the k–ε model then to the RSM model. Numerical procedure is discussed next.

4. NUMERICAL PROCEDURE

All turbulence models discussed above have been implemented in a commercial CFD code AVL SWIFT/FIRE [25]. This code employs the finite-volume discretization method. The integral form, applicable to a non-moving control volume with the outward surface (cell-face) vectors $\mathbf{A} = A_k \mathbf{i}_k$, can be written as

$$\underbrace{\frac{\mathrm{d}}{\mathrm{d}t}\int_V \rho\phi \,\mathrm{d}V}_{\text{Rate of change: } R} + \underbrace{\oint_A \rho\phi U_k \,\mathrm{d}A_k}_{\text{Convection: } C} = \underbrace{\oint_A \Gamma_\phi^{kk} \frac{\partial\phi}{\partial x_k} \,\mathrm{d}A_k}_{\text{Diffusion: } D} + \underbrace{\int_V s_\phi^V \,\mathrm{d}V + \oint_A s_{\phi k}^A \,\mathrm{d}A_k}_{\text{Sources: } S} \tag{19}$$

where a general variable $\phi(x_k, t)$ can represent either scalars, or vector and tensor field components. Here, the Cartesian co-ordinate system (x, y, z) with the unit vectors $(\mathbf{i}, \mathbf{j}, \mathbf{k})$ is used and tensor notation is employed. In the above equation, ρ is the fluid density, t is time, U_k are components of the fluid velocity vector, Γ_ϕ^{kk} is the diffusion coefficient for the variable ϕ (in this case repeated indices do not imply summation), s_ϕ^V and $s_{\phi k}^A$ are the volumetric and surface source terms, respectively. All dependent variables are stored at the geometric centre of the control volume. Both surface and volume integrals are approximated by using the integrand values that prevail at the center of the face or cell. The appropriate data structure (cell-face-based connectivity) and interpolation practices for gradients and cell-face values are introduced to accommodate an arbitrary number of cell faces. Discretized control volume equation can be written as

$$\frac{\mathrm{d}}{\mathrm{d}t}(\rho_P V_P \phi_P) + \sum_{j=1}^{n_\mathrm{f}} C_j - \sum_{j=1}^{n_\mathrm{f}} D_j = (s_\phi^V)_P V_P + \sum_{j=1}^{n_\mathrm{f}} (s_{\phi k}^A A_k)_j \tag{20}$$

where C_j and D_j are convection and diffusion transport through the face j, respectively; n_f is the number of cell-faces.

For the momentum equation ($\Phi = U_i$), the source term integrated over the surface of the control volume is given by

$$S_{\Phi,j}^A = \mu \frac{\partial U_i}{\partial x_j} - \rho\overline{u_i u_j} \tag{21}$$

$\overline{u_i u_j}$ are Reynolds stresses obtained from their own transport equation in the case of RSM or HTM models or from different assumptions depending on the model employed, e.g. Boussinesq's formula for k–ε model. Reynolds stresses can be introduced into the momentum equation using the following formulation (see also References [26, 27]):

$$\overline{u_i u_j} = \underbrace{\overline{u_i u_j}_{\mathrm{iso}}^{k-\varepsilon}}_{A:\text{source+diffusion}} + \underbrace{\overline{u_i u_j}_{\mathrm{model}} - \overline{u_i u_j}_{\mathrm{iso}}}_{B:\text{source}} \tag{22}$$

where $\overline{u_i u_j}_{\mathrm{iso}}$ is an 'isotropic' part defined by Boussinesq's formula and $\overline{u_i u_j}_{\mathrm{model}}$ are obtained from the Reynolds-stress equations.

Diffusion terms arising from the Reynolds stress definition and Bousinesq's formulation ($\overline{u_i u_j}^{k-\varepsilon}_{\text{iso}}$), can be discretized following the proposal of Przulj and Basara [28] (see also References [29–31]) by using the expression for the gradient of variable Φ given as

$$\nabla\phi_j = \overline{\nabla\phi}_j + \frac{\mathbf{A}_j}{\mathbf{A}_j\mathbf{d}_j}[(\phi_{Pj} - \phi_P) - \overline{\nabla\phi}_j \cdot \mathbf{d}_j] \tag{23}$$

where $\overline{\nabla\phi_j} = f_j\nabla\phi_j + (1 - f_j)\nabla\phi_j$ and f_j is the cell-face interpolation factor.

In the case of diffusion flux in the momentum equations, the gradient given by Equation (23) is multiplied with $\mu_{\text{eff}} = \mu_{\text{t}} + \mu_{\text{lam}}$. This term stays the same regardless of whether a k–ε model or a second-moment closure is used. Remaining differences between models and Bousinesq's formulation are then used on the right-hand side of the discretized equation (see Equation (22) and term B). This source term is accompanied by the cross-diffusion term resulting from so-called deferred correction applied to the term A in Equation (22), thus

$$D_j = \underbrace{\mu_{\text{eff}}\frac{\mathbf{A}_j^2}{\mathbf{A}_j\mathbf{d}_j}(\phi_{Pj} - \phi_P)}_{\text{normal-diffusion}} + \underbrace{\mu_{\text{eff}}\overline{\nabla\phi}_j\left(\mathbf{A}_j - \frac{\mathbf{A}_j^2}{\mathbf{A}_j\mathbf{d}_j}\mathbf{d}_j\right)}_{\text{cross-diffusion}} \tag{24}$$

In the case of the HTM model proposed here, additionally μ_{eff} is expressed as

$$\mu_{\text{eff}} = \underbrace{\mu_{\text{t}}^{c_\mu=0.09} + \mu_{\text{lam}}}_{\text{diffusion}} + \underbrace{\mu_{\text{t}}^{c_\mu=f(\overline{u_iu_j},\partial U_i/\partial x_j)} - \mu_{\text{t}}^{c_\mu=0.09}}_{\text{source}} \tag{25}$$

Equation (25) is denoted as method 2 in Figure 3, while method 1 assumes that effective viscosity is based only on the re-calculated value of C_μ, thus

$$\mu_{\text{eff}} = \mu_{\text{t}}^{c_\mu=f(\overline{u_iu_j},\partial U_i/\partial x_j)} + \mu_{\text{lam}} \tag{26}$$

Figure 3 shows, as expected, that method 2 will give a convergence rate similar to the case in which the coefficient C_μ is taken to be a constant (0.09).

A deferred correction approach is also used for the treatment of convection fluxes, thus

$$C_j = \dot{m}_j\phi_j^{\text{UDS}} + \boldsymbol{\gamma}_\phi|\dot{m}_j|\varphi_j(\phi_{P_j} - \phi_P) \tag{27}$$

where mass flux $\dot{m}_j$ is given as $\dot{m}_j = \rho\mathbf{U}_j\mathbf{A}_j$, and γ_ϕ is the blending factor between upwind differencing scheme (UDS) and higher-order scheme ($0 \leqslant \gamma \leqslant 1$). The first term (the upwind contribution) is treated implicitly, while the second, underlined term is calculated by using values from the previous iteration step and treated as an additional source. The flux limiter φ_j is given by a higher order differencing scheme used to ensure a bounded solution [28].

The rate of change (see Equation (19)) is discretized by two unconditionally stable implicit schemes, namely a first-order-accurate Euler (two-time-level) scheme and a second-order-accurate three-time-level scheme. In the case of transient calculations, it was found that the best practice for the update of C_μ is the explicit one [32], in which the values recalculated on the basis of the previous time step prevail over the entire time step. In this case, it is also important to note that the under-relaxation of C_μ can be a risky practice, since it can introduce an additional 'numerical' source of periodicity and therefore it is not recommended

(otherwise more iterations have to be performed in one time step). Contrary to the transient case, the under-relaxation of C_μ is recommended for steady-state calculations.

The overall solution procedure is iterative and is based on the SIMPLE like segregated algorithm. This algorithm effectively couples the velocity and pressure fields by converting a discrete form of the continuity equation into an equation for the pressure correction. The pressure corrections are then used to update the pressure and velocity fields so that the velocity components obtained from the solution of momentum equations satisfy the continuity equation. On non-staggered grids, a special interpolation practice is required for the face velocities [31, 33].

The turbulent kinetic energy, the dissipation rate and the Reynolds-stress equations are discretized following Equation (19) and the sources are linearized following common practices; hence, no special treatment is required. The only exception is in the case of the RSM model, with the treatment of the velocity gradients next to the wall. If the Reynolds-stress equations are integrated straight to the wall, inaccurate velocity gradients can give an enormous rise to production terms, especially in the case of a coarser grid and consequently, the convergence rate will decrease. The simple treatment has been proposed by Basara [4] to ensure reasonable values of velocity gradients by using the log-law. Thus

$$\frac{\partial U_P}{\partial n} = \frac{\sqrt{\tau_{\text{wall}}/\rho}}{\kappa \delta n} \tag{28}$$

where τ_{wall} is the wall shear stress defined with the standard wall function approach by using velocity at the near wall cell parallel to the wall U_P. A 'very near' wall velocity can be derived, whose gradient satisfies Equation (29), thus

$$|\mathbf{U}_{\text{wall}}| = |\mathbf{U}_P| - \frac{1}{\kappa}\sqrt{\tau_{\text{wall}}/\rho} \tag{29}$$

By using a co-ordinate transformation to obtain Cartesian velocity components, production stress terms can be updated with the velocity gradients which fit to the 'log-law' velocity gradient in the direction normal to the wall. Such predicted Reynolds stresses, when introduced into the momentum equations fit much better to the wall stresses predicted from wall functions. Otherwise very fine grid distribution near the wall is required to obtain smooth velocity profiles on the wall. Furthermore, the production of turbulence kinetic energy can now be obtained by summing up the production stress terms and then compared with the production term obtained from the log-law in order to provide a correction factor which is then used to correct a stress production terms in Reynolds stress equations (more details are given in the work of Basara, 2002).

The linearized algebraic equations are solved by very efficient, preconditioned conjugate gradient methods. The symmetric gradient method is used to solve equations with the symmetric matrix and the biconjugate method (Bi-CGSTAB) of van der Vorst [34] for equations with an asymmetric matrix. Both methods are used with an incomplete Cholesky preconditioning technique (see Reference [35]).

Calculations on different grids with different differencing schemes are a prerequisite for reliable simulations. Otherwise, numerics may introduce errors which could obscure turbulence model performances. As shown above, all terms in equations are discretized with minimum second-order accuracy. Furthermore, calculations presented in the next sections have been

performed on very fine numerical grids. Altogether, this ensures that all results presented in this paper are grid independent. Also, the benchmarks chosen for this paper are very well known and well documented in many references and hence, it is possible to make comparisons with many other previously reported calculations even performed with the same models (some of the cases were included in ERCOFTAC Workshops).

5. ILLUSTRATION OF MODEL PERFORMANCE: HTM AND ITS PHYSICAL IMPLICATIONS

The performance of the hybrid turbulence model obviously depends on the Reynolds-stress closure used. Therefore, it is not expected that the HTM will perform better than the RSM model, but that the results will lie somewhere between the RSM and k–ε models results. Nevertheless, there are several very important flow categories, where the application of the HTM, unlike the k–ε model scheme, captures some very important flow phenomena. Furthermore, for all cases presented below, overall differences between convergence rates are similar to that shown in Figure 3.

It is very well known, that the eddy–viscosity modelling concept exhibits a number of weak points. The most known model scheme from this group, being most widely used in industrial praxis, is the standard linear k–ε model. The original model formulation for ν_t [5] represents the proportionality between the turbulent shear stress component ($\rho\overline{uv}$) and the mean shear ($\partial U/\partial y$), in analogy to the viscosity law. This model was subsequently put into the tensor form and extended for $2\delta_{ij}k/3$ (see Equation (2)) to ensure that $\overline{u_i u_i} = 2k$. Whereas its performance could be regarded as acceptable in the flows being dominated by the mean shear, it fails to capture important flow features in most of the flows departing from the thin shear layer approximation: flows influenced by streamline curvature and strong pressure gradients causing high acceleration and deceleration, swirling flows, separating and reattaching flows, flows with stagnation regions, etc. The performances of the HTM model in some of these flow classes are illustrated as follows.

5.1. *Round jet impinging onto a flat plate*

In the hybrid turbulence model scheme, the kinetic energy of turbulence is obtained from modelled Reynolds-stress equations, implying the application of the exact expressions for the stress generation. The resulting expression for the production of the kinetic energy of turbulence for the 2D flows reads

$$P_k = \frac{1}{2}(P_{11} + P_{22} + P_{33}) = -\overline{u^2}\frac{\partial U}{\partial x} - \overline{uv}\left(\frac{\partial U}{\partial y} + \frac{\partial V}{\partial x}\right) - \overline{v^2}\frac{\partial V}{\partial y} \tag{30}$$

The superiority of such a procedure becomes especially illustrative when comparing this expression with the appropriate formulation used in the framework of the k–ε modelling concept:

$$P_k = 2\mu_t\left(\frac{\partial U}{\partial x}\right)^2 + \mu_t\left(\frac{\partial U}{\partial y} + \frac{\partial V}{\partial x}\right)^2 + 2\mu_t\left(\frac{\partial V}{\partial y}\right)^2 \tag{31}$$

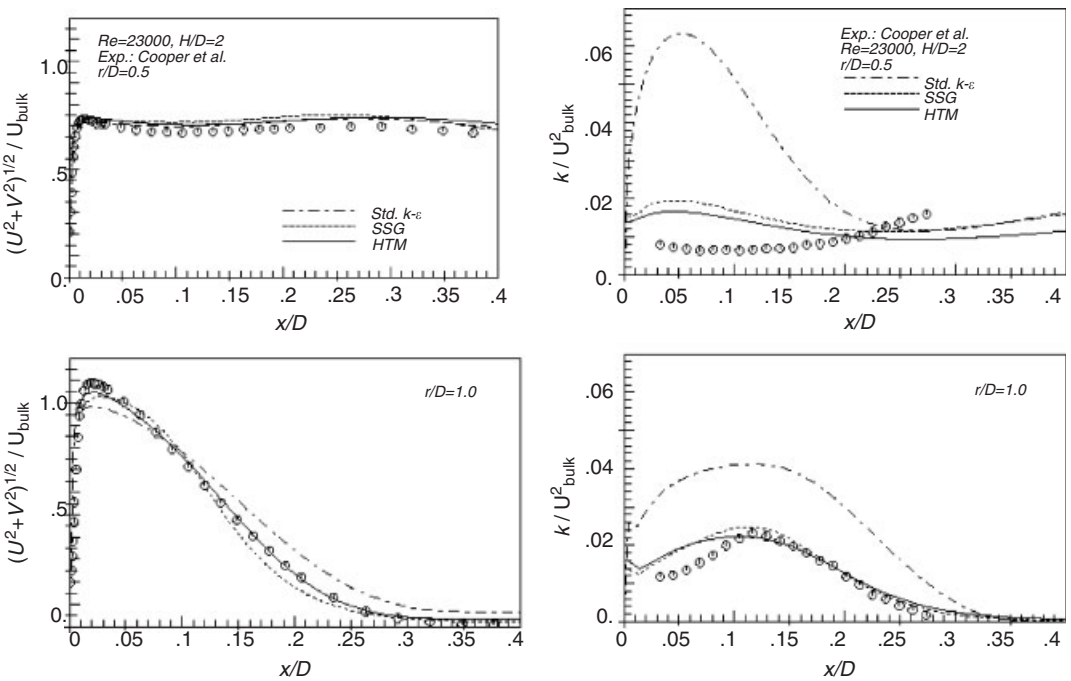

Figure 4. Profiles of the resultant mean velocity and turbulent kinetic energy in the stagnation region of the flow impinging normally onto a flat wall.

In thin shear flows dominated by the mean shear ($\partial U/\partial y$), both formulations result in approximately the same value, because effects of the normal straining are neglected. However, in flows with a more complex mean rate of strain tensor S_{ij}, whose components exhibit different levels and signs, the production rates are likely to be different. The formulation for P_k in the framework of the k–ε model always gives a positive production rate, displaying no dependence on the sign of the individual strain tensor components. A typical flow example illustrating such a behaviour is the jet impinging perpendicularly onto a flat plate [36], imposing a negative $S_{11} = \partial U/\partial x$ (deceleration) and a positive $S_{22} = \partial V/\partial y$ (acceleration in the vertical co-ordinate direction) in the impingement (stagnation) region, with $\overline{v^2} > \overline{u^2}$. Contrary to the exact formulation for P_k used within the RSM concept, this irrotational straining contributes strongly to the excessive production of the kinetic energy of turbulence in the k–ε modelling framework, Figure 4. Due to the fact that this flow is pressure dominated, the influence of k on the mean velocity is not very pronounced, nevertheless an overpredicted k value would lead to an overestimation of the heat transfer rate in this region. The results obtained by the present hybrid turbulence model are fully compatible with the Reynolds-stress closure results. The impinging jet case belongs to the category of the flows influenced locally by the streamline curvature, which in fact implies additional effects on the kinetic energy production rate through an extra strain rate $(U^2/R)\mathbf{n}_\sigma$, where U stands for the velocity component tangential directed to the streamline—$U\mathbf{t}$, $\mathbf{n}_\sigma = R\,\mathrm{d}\mathbf{t}/\mathrm{d}\sigma$ denotes direction normal to $\mathbf{t}$ and R is the radius of the streamline curvature.

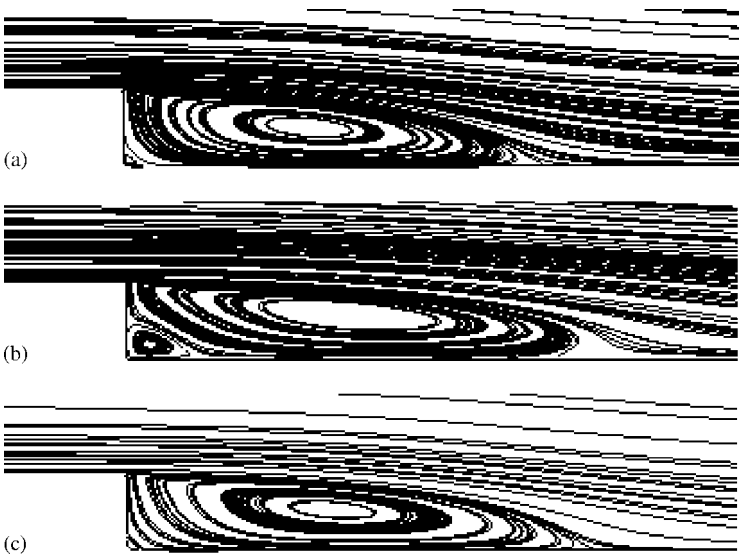

Figure 5. Streamline patterns of the flow over a backward-facing step obtained by (a) standard k–ε model, (b) RSM and (c) HTM.

5.2. *Flow over a backward-facing step*

The next example with local streamline curvature is the flow over a backward-facing step, separating at the sharp edge of the step and creating a separation bubble behind the step. A case studied experimentally [37] and by means of DNS [12] was computed. Figure 5 displays the streamline patterns obtained by the standard k–ε model, the SSG RSM and the hybrid model scheme proposed. Apart from the anomaly related to reverse curvature of the mean dividing streamline at reattachment, causing in fact a certain shortening of the separation region from the experimental $X_r/H = 6.1$ to the computational $X_r/H = 5.55$, the RSM gives a large recirculating zone, in accordance with the reference data. The RSM traditionally reproduces a lower level of the turbulent shear stress $\overline{uv}$ and a lower kinetic energy of turbulence k along the shear layer aligned with the mean dividing streamline, than those computed by the k–ε model (not shown here). These damping effects on turbulence imposed by streamline curvature are captured by the RSM, in contrast to the k–ε model. A lower level of the shear stress implies a reduction of the fluid entrainment into the shear layer and an extension of the recirculation bubble. The results using the hybrid turbulence model exhibit a similar behaviour, resulting in $X_r/H = 6.03$, which is substantially longer than the result using the k–ε model ($X_r/H = 5.47$), Figure 5. It is interesting to note in Figure 5 that the hybrid turbulence model does not capture a small, counter-rotating vortex at the base of the step, the same discrepancy as in the predictions with the standard k–ε model. These secondary currents are stress induced, resting on the selective influence of the anisotropic Reynolds-stress field on the mean flow. Therefore, this feature is beyond the reach of the hybrid modelling procedure, because of the eddy–viscosity-based coupling of the Reynolds stress with the mean velocity fields. However, this feature can be captured by a low-Reynolds number model, accounting for the interaction

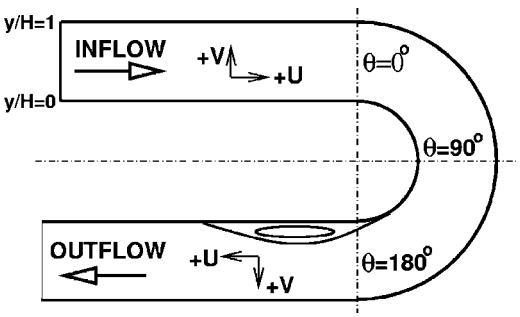

Figure 6. Schematic of the 180° turned U-band.

within the viscous sublayer and the reminder of the flow domain (not shown here). On the other hand, the HTM does not exhibit an unrealistic rearward streamline curvature at the end of separation, something very common for the predictions with RSM models (see e.g. the work of Hanjalic and Jakirlic [38]).

5.3. *Flow in a* 180° *turned U-bend*

Besides the local streamline curvature, the flow can be curved as a whole by the imposed boundaries, as illustrated by the next example, the 180° turned U-bend, Figure 6 (Exp.: Reference [39]). It represents the flow class affected by the so-called longitudinal streamline curvature. This flow configuration is characterized by an increase in the mean flow angular momentum with radius of curvature, reaching its highest value in the part of the flow over the convex surface. The additional strain rate originating from the streamline curvature attenuates the turbulence in this flow region (*stabilizing curvature*). On the other hand, it amplifies the turbulence in the opposite situation, i.e. in the part of the flow over the concave surfaces (*destabilizing curvature*). It is illustrated in Figure 7, showing profiles of the mean velocity and kinetic energy of turbulence at selected location across the curved part of the flow (prior to the separation bubble) and the recirculating region itself. Whereas the RSM and HTM reproduce very well the turbulence attenuation over the inner surface of the U-bend, corresponding to the flow acceleration, and the turbulence amplification over its outer surface, corresponding to the deceleration of the flow, the standard k–ε model results in a fully symmetric profile of the k in spite of the correctly predicted asymmetrical profile of the mean velocity, Figure 7(a). Such a high turbulence level completely prevents flow separation, a fact depicted in Figure 8, showing the streamline patterns obtained by all three model schemes. The application of both the RSM and HTM closures results in a separation zone, whose onset is placed at the end of the U-band. The mean velocity profiles within the separation zone are shown in Figure 7(b), indicating a somewhat thicker recirculation bubble obtained by the RSM.

5.4. *Swirling flow in an axially rotating pipe*

The next flow example investigated is the fully developed flow in an axially rotating pipe (DNS: Reference [40]), being representative of the confined swirling flows. Besides the strong

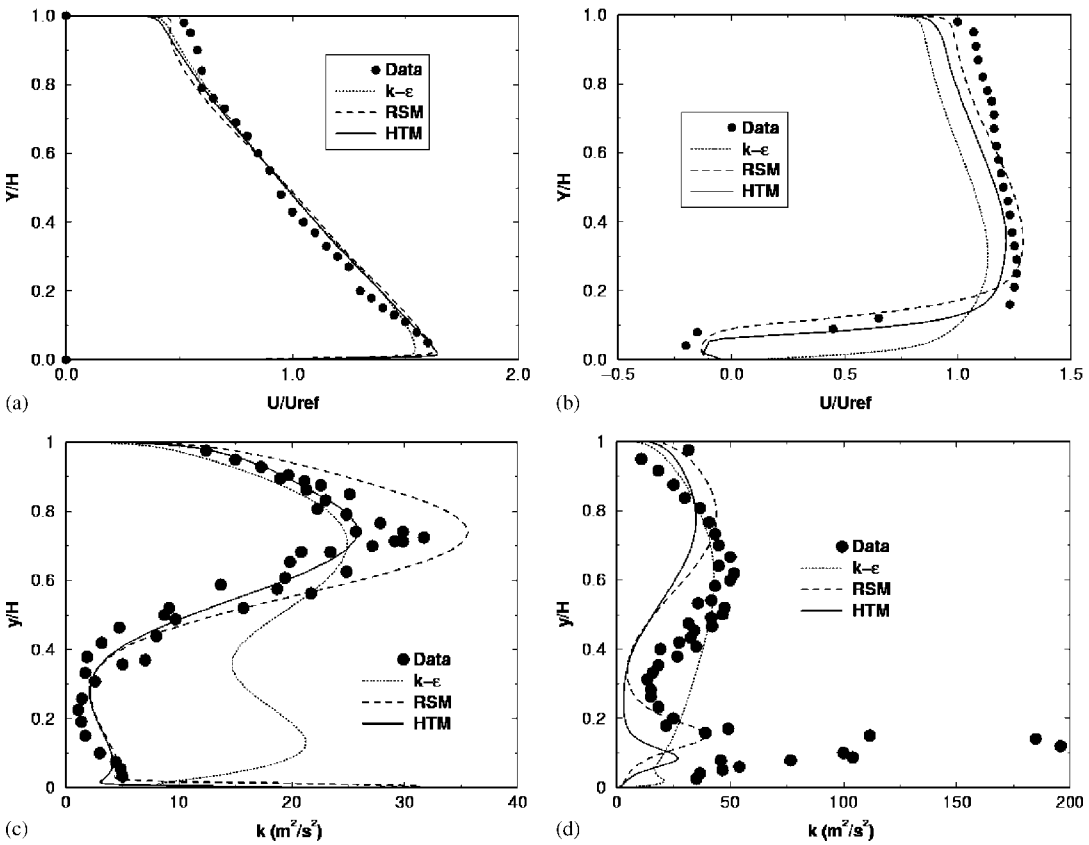

Figure 7. Mean velocity and kinetic energy profiles at two selected locations along the flow in a 180° turned U-band, (a) and (b) at 90° and (c) and (d) at 180°.

mean ($\partial U/\partial r$) and secondary ($\partial W/\partial r$) shear strainings, the flow is strongly affected by the streamline curvature, being represented through an additional strain $-W/r$. In spite of being computationally treated as unidirectional, i.e. one dimensional ($\partial/\partial z$, $\partial/\partial\varphi = 0$), this configuration displays all features of a three-dimensional flow, necessitating solution of the transport equation for all three velocity components ($U_r, U_\varphi, U_z \equiv V, W, U$) and all six non-zero Reynolds-stress components. Rotating and swirling effects impose a strong anisotropy on the eddy viscosity field. Eddy viscosity has no longer an isotropic, scalar nature, as enforced by the k–ε model formulation, but a tensorial one. It is characterized by a strongly anisotropic behaviour of its components: $\nu_{t,12} = -\overline{uv}/(\partial U/\partial r)$, $\nu_{t,23} = -\overline{vw}/[r\partial(W/r)/\partial r]$ and $\nu_{t,13} = -\overline{uw}/(\partial W/\partial r)$ (see e.g. Reference [41]). Although the background Reynolds-stress closure is inherently capable of accounting for such a behaviour, it is the coupling between the velocity and Reynolds-stress field via Boussinesq's ansatz, which does not allow any other solution for the circumferential velocity component except the profile indicating the solid body rotation: $W/W_{\text{wall}} = r/R$, Figure 9(b). This fact can be illustrated by writing the φ-component of the momentum equation with the $\overline{vw}$-shear stress being defined by the Bousinesq's formula

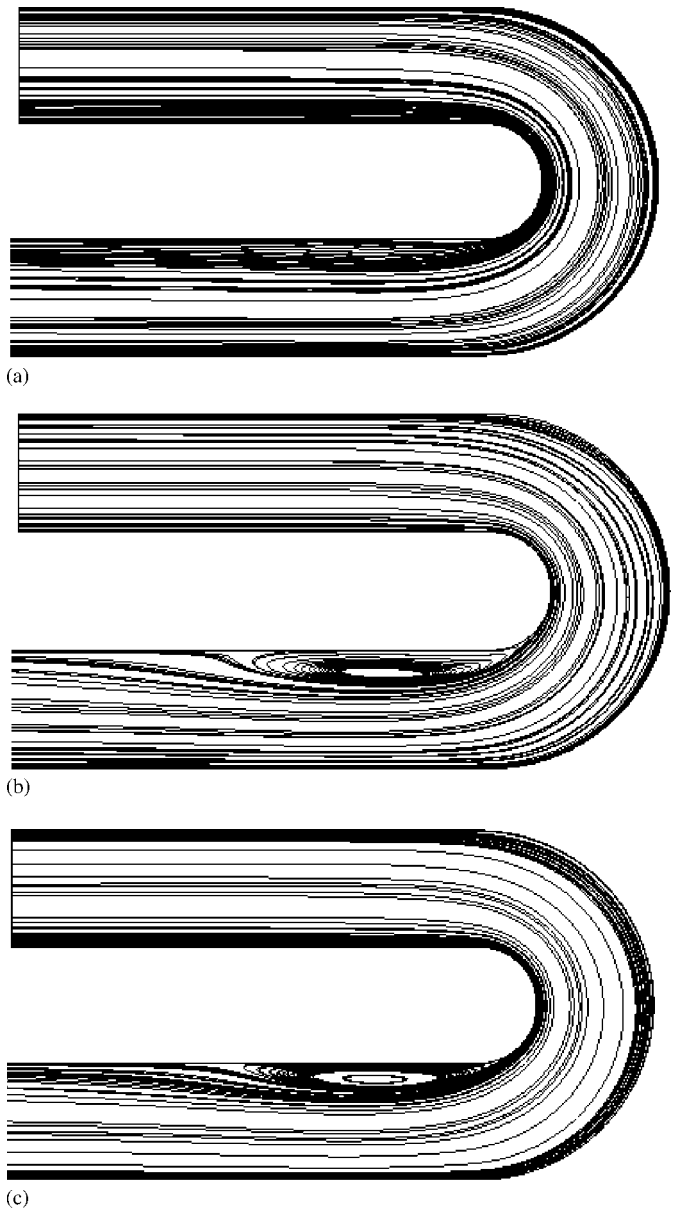

Figure 8. Streamline patterns of the flow in 180° turned U-band obtained by (a) standard k–ε model (b) RSM and (c) HTM.

$(-\overline{vw} = v_t r \partial(W/r)/r)$:

$$0 = \frac{1}{r^2}\frac{\partial}{\partial r}\left\{r^2\left[\nu r\frac{\partial}{\partial r}\left(\frac{W}{r}\right) - \overline{vw}\right]\right\} \Rightarrow 0 = (\nu + \nu_t) r \frac{\partial}{\partial r}\left(\frac{W}{r}\right) \tag{32}$$

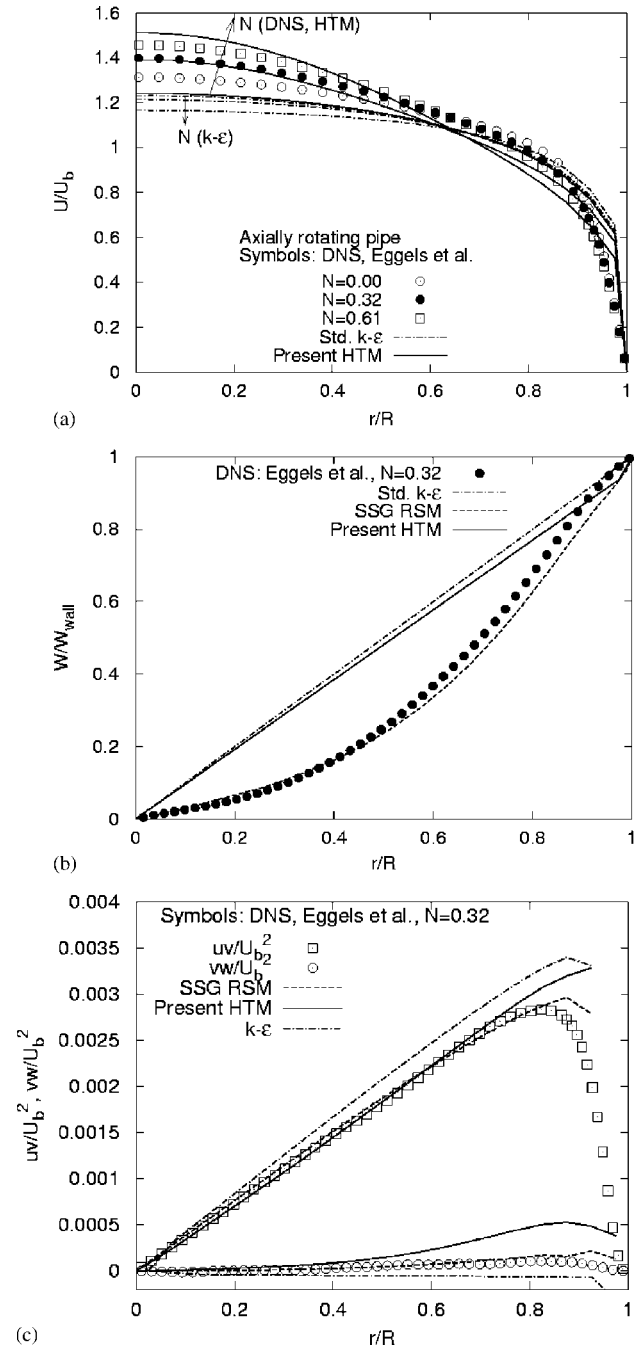

Figure 9. (a) Axial and (b) circumferential velocity components and (c) shear-stress components in the fully developed flow in an axially rotating pipe.

Independent of the model for the turbulent viscosity ν_t, this equation can be satisfied only if $W \propto r$. This equation is coupled with the equation governing the axial velocity U via the turbulence quantities only ($-\overline{uv} = \nu_t \partial U/\partial r$):

$$0 = \frac{1}{r}\frac{\partial}{\partial r}\left[r\left(\nu\frac{\partial U}{\partial r} - \overline{uv}\right)\right] - \frac{1}{\rho}\frac{\partial P}{\partial z} \Rightarrow 0 = \frac{1}{r}\frac{\partial}{\partial r}\left[r(\nu + \nu_t)\frac{\partial U}{\partial r}\right] - \frac{1}{\rho}\frac{\partial P}{\partial z} \tag{33}$$

Figure 9(c) shows both shear stresses computed by all three model schemes. The Boussinesq's correlation results in a wrong (compared to the DNS data), slightly negative value of the $\overline{vw}$-shear stress and a high value of the $\overline{uv}$-shear stress, being even higher than in the non-rotating case (not shown here). This high shear stress prevents an increase in the centreline velocity U_C by increasing the rotational intensity N, which traditionally indicates a laminar like behaviour of the axial velocity components. The U_C-value is even slightly decreased (see direction in Figure 9(a) indicated by the arrow), exhibiting in fact no sensitivity of the k–ε model to rotational effects. Contrary to that, the HTM accounts for this effect in accordance with the DNS data and the RSM results (not shown here). Responsible for such a behaviour is the decreasing level of the turbulent viscosity i.e. shear stress by the increasing N, Figure 9(c). The functional dependency for C_μ plays a very important role here, exhibiting a much lower level than 0.09, Figure 2. This successful capturing of the axial velocity component is very important, particularly for swirling flows in short combustor geometries, where the flame stabilization is reached by the vortex break-up, creating a flow reversal in the core region. This free bubble is traditionally missed by applying the k–ε model.

5.5. *Flow around a car model—Ahmed body*

The Ahmed body, a three-dimensional idealized vehicle model represents the key benchmark for validation of the turbulence models regarding external car aerodynamics. This case allows investigation of the back slant effect on the overall drag force. At a certain angle of the slant, a vortex breakdown phenomena appears, causing the sudden pressure drop acting on the model. Basara and Alajbegovic [42] showed that only transient calculation is appropriate for such a simulation, since vortex shedding is present. However, the aim here was only to check if the HTM provides results lying between the RSM and the k–ε model, as presented above for several two-dimensional flows (see Reference [32], for performances of the HTM model for the vortex-shedding flow). The case with the back slant angle of 35° is calculated here, since the flow detaches on the edge, hence, the separation point is not significantly influenced by transient effects.

The computational domain contains 523 000 hexahedral cells (see Figure 10). Local grid refinement is applied to improve a grid resolution around the body. The grid is carefully checked for the numerical error by employing different differencing schemes and it represents the minimum size acceptable for turbulent models testing. The first next to the wall cells ensure y^+ values on the body to be in the range between 20 and 50. Attention was also given to the boundary conditions. Measured velocity profile was used for extrapolation at the inlet boundary faces. A minimum inlet distance from Ahmed body has been validated and it was found that 0.5 m is sufficient in order not to influence results. The best agreement was achieved when the inlet profile was taken from the same set of measurements used for comparisons (inlet profile was taken from $x = -1.443$ m, Reference [43]).

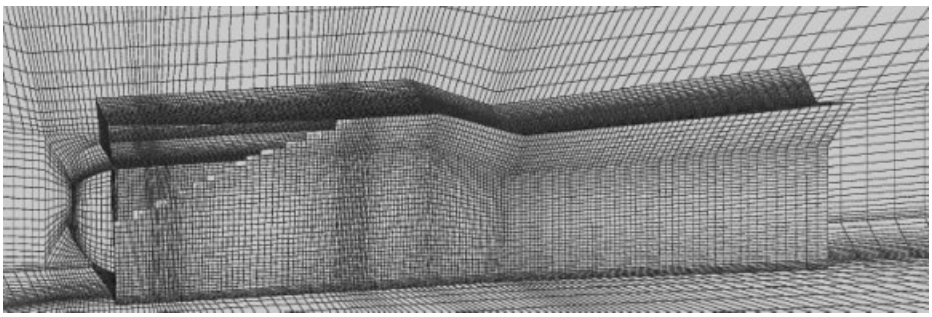

Figure 10. Calculation grid for the Ahmed body.

The selected mean velocity and turbulent stress profiles at the symmetry plane are displayed in Figure 11 at selected locations within the back slant region and the car body wake. Both the streamwise and normal (not shown here) velocity components are captured well at all locations with all models applied. The streamwise and shear stress components reproduced by the full RSM are in closest agreement with the measurements, though the other model results are not in larger discrepancy with the measured data. A small difference between results obtained by both RSM and HTM is understandable, keeping in mind that the same Reynolds stress equations are used to simulate turbulence field. Predicted surface streamlines with the HTM and RSM models are shown in Figure 12. A noticeable difference has been observed but it has to be kept in mind, that the complete rear part of the car body is in the separation region starting near the top edge. Therefore, the same basic flow pattern has been predicted with all models, including the k–ε model.

6. TOWARDS A LOW-REYNOLDS NUMBER, HTM

The immediate wall vicinity is characterized by a number of mean flow and turbulence phenomena. Besides the strong viscous effects, damping uniformly the turbulence fluctuations in all directions, turbulence structure is significantly influenced by the non-viscous, directionally biased wall-blockage effects, imposing a different level of damping on the individual velocity fluctuation components. This results in an appropriate eddy flattening, causing a high level of anisotropy of both, the Reynolds stress and dissipation rate tensors. Different flows, being characterized by different extra-strain rates, display a different anisotropy level. Whereas a favourable pressure gradient (flow acceleration) promotes anisotropy, an imposed adverse pressure gradient (flow deceleration) acts towards an isotropic state. The second-moment closures are inherently capable of accounting for all the effects mentioned above. Both, large energy containing structures and dissipative small-scale motion, as well as their interaction with the mean flow, are simulated adequately by corresponding terms in the transport equations for turbulent stresses. Suitable model parameters, such as Reynolds stress and dissipation rate anisotropy invariants, as well as the Reynolds number of turbulence, are usually introduced to accommodate the near-wall effects in modelling these terms. In the framework of the standard, linear k–ε modelling concept, a damping function f_μ, multiplying the turbulent

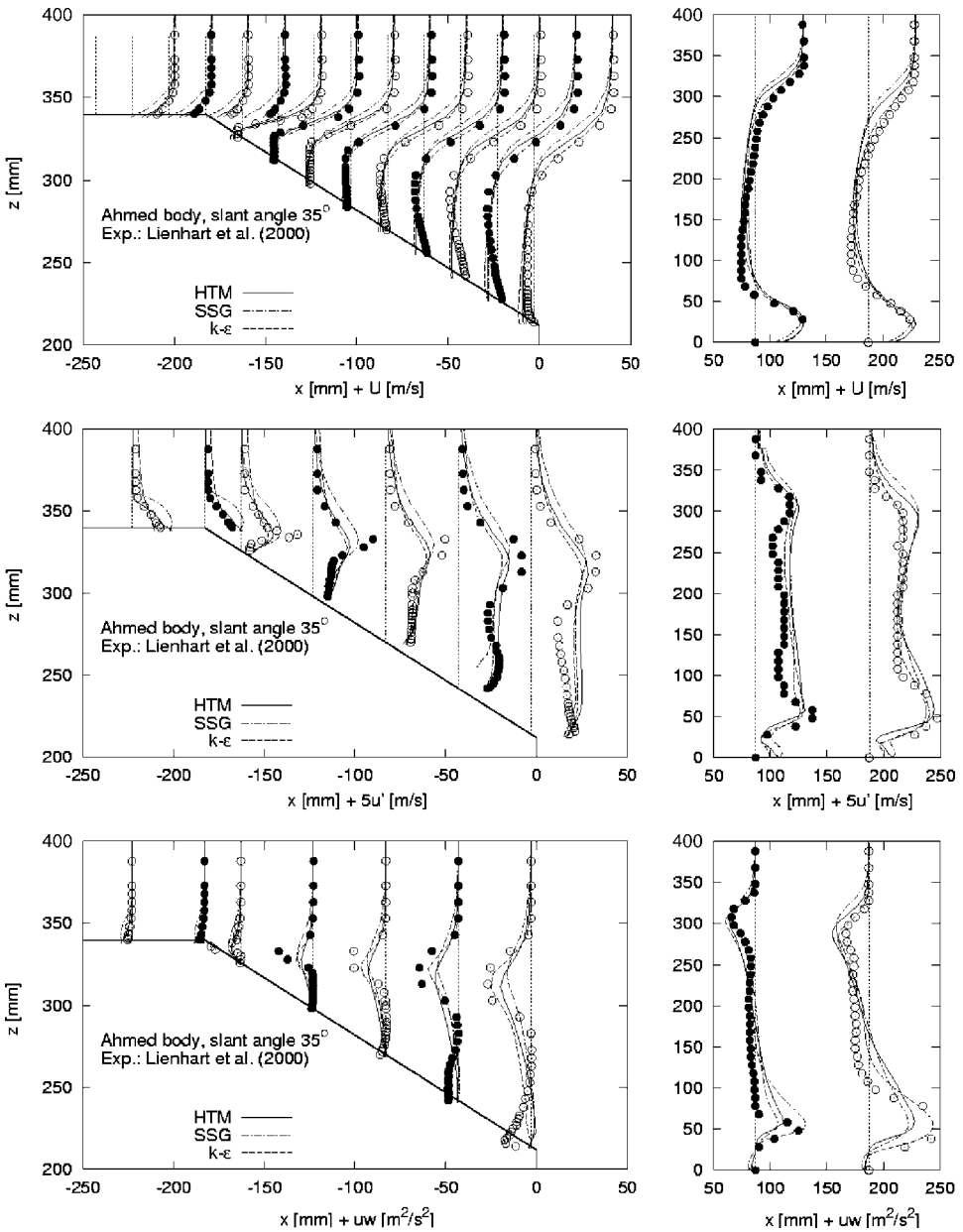

Figure 11. Streamwise mean velocity components (upper), streamwise turbulence intensities (middle) and turbulent shear stresses (lower) at selected locations within the back slant region (left) and wake region (right) of the Ahmed body.

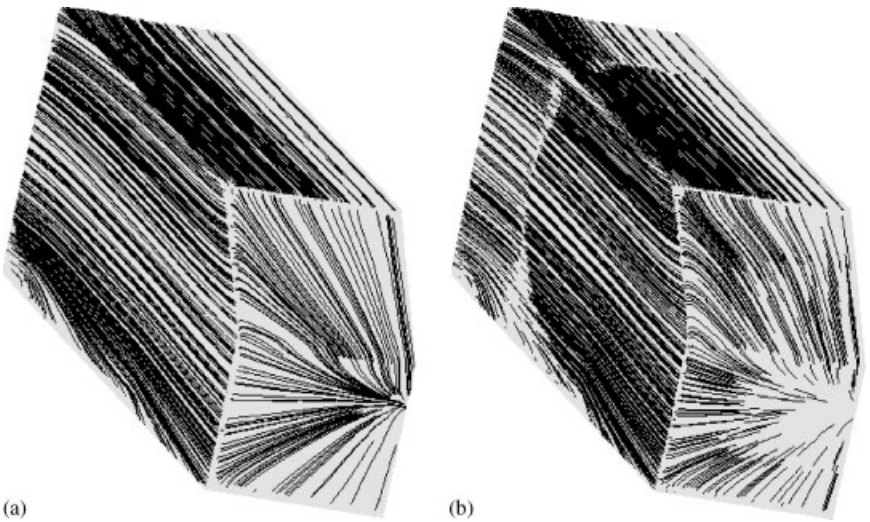

Figure 12. Surface streamlines predicted by (a) HTM and (b) RSM.

viscosity, is traditionally introduced to mimic the near-wall behaviour mentioned:

$$\nu_t = C_\mu f_\mu \frac{k^2}{\varepsilon} \tag{34}$$

The function f_μ should provide a vanishing turbulent viscosity by approaching the solid wall. On the other hand, this damping function takes a value of unity in the fully turbulent region, matching usually the logarithmic layer. Most model developers formulate this function in terms of the wall distance (see e.g. Reference [44]), exploiting the fact that the scaling of the near-wall turbulence structures corresponds approximately to the local wall distance. Besides its insensitivity to some very important flow phenomena (e.g. transitional phenomena), the wall distance is an extremely poorly defined model parameter in the case of very complex flow geometries with multiple walls. A much more suitable model parameter is the turbulence Reynolds number $Re_t = k^2/(\nu\varepsilon)$, which traditionally represents the viscosity effects, see e.g. Reference [45]. On the other hand, this function cannot account for the stress anisotropy in the framework of the two-equation k–ε model and this reflects the most important weakness of this modelling concept. Durbin [46] proposed a new model for turbulent viscosity accounting for both, viscous effects and Reynolds-stress anisotropy:

$$\nu_t = 0.23\overline{v^2} \max\left[6.0\left(\frac{\nu}{\varepsilon}\right)^{1/2}; \frac{k}{\varepsilon}\right] \tag{35}$$

The viscosity effects are modelled by the time scale switch between the Kolmogoroff time scale $\tau_K = (\nu/\varepsilon)^{1/2}$ and the turbulent time scale k/ε (the turbulence Reynolds number could be interpreted as the square of the ratio of the turbulent time scale to the Kolmogoroff time scale). Recognizing that the wall imposes a selective damping on the normal-to-the-wall velocity fluctuation, contributing strongly to the increased turbulence anisotropy by approaching the two-component state very close to the wall, Durbin introduced the normal stress component

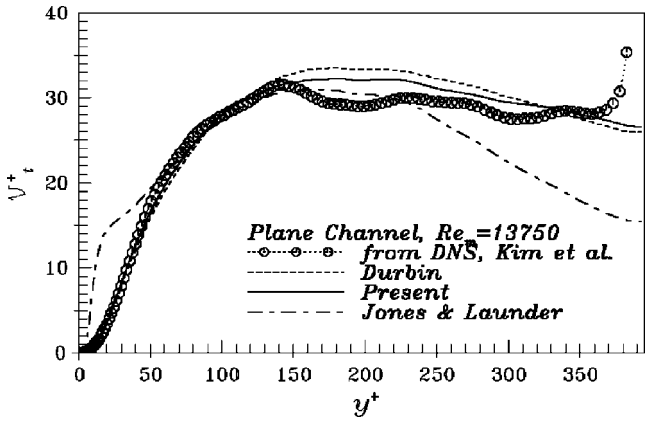

Figure 13. Profile of the turbulent viscosity across the flow in a plane channel.

as a most suitable measure of the kinematic wall blockage. This variable is obtained from its own transport equation within the framework of the Durbin's three-equation model (k–ε–$\overline{v^2}$). The profile of the eddy viscosity across the fully developed channel flow obtained from Equation (2) by feeding in the DNS data of Kim *et al.* [47] for k, ε and $\overline{v}^2$ agrees very well with the DNS results for $v_t = -\overline{uv}/(\partial U/\partial y)$, Figure 13. For the sake of comparison, the results obtained by Jones and Launder's low-Reynolds number k–ε model formulation are also depicted. In the hybrid modelling strategy all turbulent stress components are available and the Durbin's formulation for v_t could be applied. However, unlike Durbin's $\overline{v^2}$, standing for a scalar without direction of preference, the $\overline{v^2}$—stress obtained from the background second-moment closure represents generally a Cartesian stress component being directed into the y-co-ordinate axis. We adopted here a formulation which employs the switch between the Kolmogoroff length scale $\eta_K = (v^3/\varepsilon)^{1/4}$ and the turbulent length scale $k^{3/2}/\varepsilon$. The stress anisotropy is accounted for by the Lumley's two-componentality parameter A ($A = 1 - 9(A_2 - A_3)$, $A_2 = a_{ij}a_{ji}$, $A_3 = a_{ij}a_{jk}a_{kl}$, $a_{ij} = \overline{u_iu_j}/k - 2\delta_{ij}/3$):

$$v_t = 0.144Ak^{1/2} \max\left[10\left(\frac{v^3}{\varepsilon}\right)^{1/4}; \frac{k^{3/2}}{\varepsilon}\right] \tag{36}$$

The radial profile of v_t obtained with this formulation shows very good agreement with Durbin's model and appropriate DNS data for the turbulent flow in a plane channel. Furthermore, this formulation also satisfies the asymptotic behaviour of v_t in approaching the solid wall ($v_t \sim y^3$), unlike the model of Durbin ($v_t \sim y^4$).

The computational performance of the present low Reynolds-number HTM involving this formulation for v_t is tested in the fully developed turbulent channel flow. The presently adopted background low Reynolds number second-moment closure model is that of Hanjalic and Jakirlic [38] here denoted as HJ low-Re RSM. This model was previously validated very intensively in a broad variety of turbulent flows, featuring different mean flow and turbulence phenomena. Figure 14 shows semi-log plots of the mean velocity profiles for a range of the bulk Reynolds numbers between 2980 and 123.200 exhibiting excellent agreement with

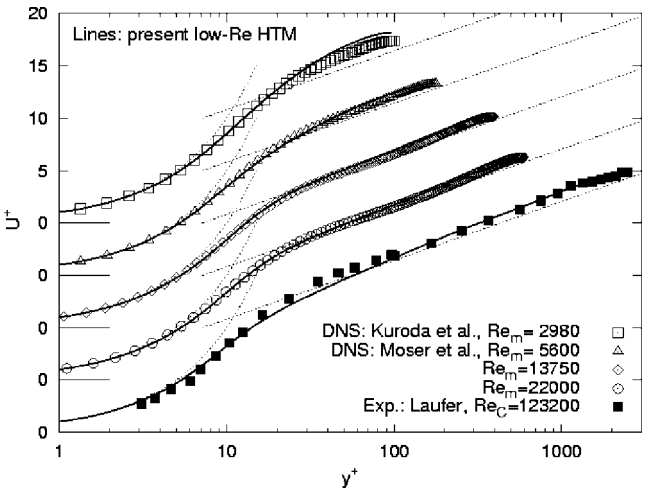

Figure 14. Semi-log plots of the mean velocity for a range of the bulk Reynolds number in the fully developed turbulent channel flow.

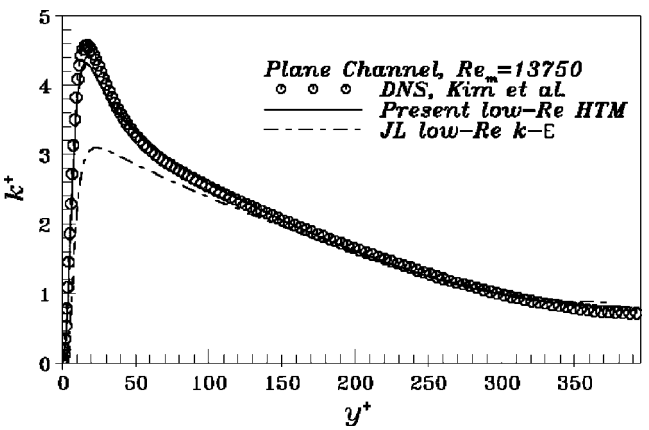

Figure 15. Turbulent kinetic energy profile across the fully developed turbulent channel flow.

available DNS [10, 48] and experimental results [49]. Figure 15 displays very good agreement of the turbulent kinetic energy resulting from the background low-*Re* RSM with the DNS results. The results obtained by the Jones and Launder low-*Re* Reynolds number k–ε model are also shown.

The purpose of the presented results was to indicate the potential of the low-Reynolds-number hybrid modelling procedure. Further analysis and model validation are necessary. Other low-Reynolds-number second-moment closure schemes can also be adopted.

7. CONCLUSIONS

The main conclusion drawn from this study is that the 'hybrid' turbulence strategy improves the predictions comparing to simpler eddy–viscosity turbulence models. It is shown that Boussinesq's relation can provide a good solution if the turbulence is modelled via Reynolds-stress equations and the constant value for C_μ is replaced with a variable formulation. An implementation of models used for calculations is described in order to provide the arguments that the proposed model is a compromise between the accuracy of RSM and the robustness of the k–ε model. The HTM model can also be applied as an 'initialization' model, used between the k–ε and RSM models in order to stabilize and shorten RSM calculations. Moreover, the main benefits from this modelling strategy should be expected in complex industrial calculations, especially in flows where overprediction of turbulent kinetic energy caused by the inadequate modelling approach of the k–ε model departs largely from the real situation. Furthermore, the potential of the hybrid modelling strategy for predicting the flow in the near-wall region is also investigated by considering fully developed channel flow in a large range of the bulk Reynolds numbers, extending further its field of application.

ACKNOWLEDGEMENTS

The authors gratefully acknowledge the many fruitful discussions and valuable suggestions of Prof. K. Hanjalic (Delft University of Technology). S. Jakirlic acknowledges the financial support of the Deutsche Forschungsgemeinschaft (SFB568).

REFERENCES

1. Bradshaw P. The best turbulence models for engineers. In *Modeling Complex Turbulent Flows*, Salas *et al.* (eds). Kluwer Academic Publishers: Dordrecht, 1999; 9–28.
2. Lebrere L, Buffat M, Le Penven L, Dillies B. Application of Reynolds stress modeling to engine flow calculations. *ASME Journal of Fluids Engineering* 1996; **118**:710–720.
3. Apsley DD, Leschziner MA. Advanced turbulence modelling of separated flow in a diffuser. *Flow, Turbulence and Combustion* 1999; **63**:81–112.
4. Basara B. Computations of automotive flows using the second-moment closure. *Proceedings of ECCOMAS 2000*, Barcelona, Spain, 11–14 September.
5. Boussinesq J. Theorie de l'ecoulement tourbillant. *Memoires presentes par diverse savans a l'academie des sciences de l'institut de France*, vol. 23, No. 46 Paris, 1877.
6. Baldwin BS, Lomax. Thin layer approximation and algebraic model for separated turbulent flows. *AIAA Paper No.* 78-257, 1987.
7. Rodi W, Mansour NN, Michelassi V. One-equation near-wall turbulence modelling with the aid of DNS data. *ASME Journal of Fluids Engineering* 1993; **115**:196–205.
8. Spalart PR, Allmaras SR. A one-equation turbulence model for aerodynamic flows. *La Recherche Aerospatiale* 1994; **1**:5–21.
9. Shur ML, Strelets MK, Travin AK, Spalart PR. Turbulence modelling in rotating and curved channels: assessing the Spalart-Shur correction. *AIAA Journal* 2000; **38**(5):784–792.
10. Moser RD, Kim J, Mansour NN. Direct numerical simulation of turbulent channel flow up to $\mathrm{Re}\tau = 590$. *Physics of Fluids* 1999; **11**(4):943–945.
11. Orlandi P, Fatica M. Direct simulations of a turbulent pipe rotating around its axis. *Journal of Fluid Mechanics* 1997; **343**:43–72.
12. Le H, Moin P, Kim J. Direct numerical simulation of turbulent flow over a backward-facing step. *Journal of Fluid Mechanics* 1997; **330**:349–374.
13. Launder BE, Spalding DB. The numerical computation of turbulent flows. *Computer Methods in Applied Mechanics and Engineering* 1974; **3**:269–289.
14. Speziale CG, Sarkar S, Gatski TB. Modeling the pressure–strain correlation of turbulence, an invariant dynamical systems approach. *Journal of Fluid Mechanics* 1991; **227**:45–272.

15. Gibson MM, Launder BE. Ground effects on pressure fluctuations in the atmospheric boundary layer. *Journal of Fluid Mechanics* 1978; **86**:491–511.
16. Lien FS, Leschziner MA. Second-moment modelling of recirculating flows with a non-orthogonal collocated finite-volume algorithm. In *Turbulent Shear Flows*, vol. 8, Durst *et al*. (eds). Springer: Berlin, 1993; 205–222.
17. Prandtl L. Über ein neues Formelsystem für die ausgebildete Turbulenz. *Nachrichten von der Akademie der Wissenschaft*, Göttingen, Mathematisch-physikalische Klasse, 1945; 6–19.
18. Hinze JO. *Turbulence*. McGraw Hill: New York, 1959.
19. Pope S. A perspective on turbulence modelling. *Modeling Complex Turbulent Flows*, Salas *et al*. (eds). Kluwer Academic Publishers: Dordrecht, 1999; 53–67.
20. Cazalbou JB, Bradshaw P. Turbulent transport in wall bounded flows. Evaluation of model coefficients using direct numerical simulation. *Physics of Fluids A* 1993; **5**(12):3233–3239.
21. Rodi W. Turbulence models and their applications in hydraulics—A state of the art review. *Technical Report*, University of Karlsruhe, Karlsruhe, Germany, 1980.
22. Pourahmadi F, Humphrey JAC. Prediction of curved channel flow with an extended k–ε model of turbulence. *AIAA Journal* 1983; **21**(10):1365–1373.
23. Barakos G, Drikakis D. Numerical simulation of transonic buffet flows using various turbulence closures. *International Journal of Heat and Fluid Flow* 2000; **21**:620–626.
24. Lilly DK. A proposed modification of the Germano subgrid-scale closure model. *Physics of Fluids A* 1992; **4**(3):633–635.
25. AVL AST. Swift Manual 3.1, AVL List GmbH, Graz, Austria, 2002.
26. Basara B. A numerical study into the effects of turbulent flows around full-scale buildings. *Ph.D. Thesis*, City University of London, UK, 1993.
27. Basara B. Two-layer model combining the Reynolds-stress model with the low *Re*-number k–ε model near the wall. *ASME Paper* 1998-4896, 1998.
28. Przulj V, Basara B. Bounded convection schemes for unstructured grids. *AIAA Paper* 2001-2593, 2001.
29. Muzaferija S. Adaptive finite volume method for flow predictions using unstructured meshes and multigrid approach. *Ph.D. Thesis* Imperial College, University of London, UK, 1994.
30. Demirdzic I, Muzaferija S. Numerical method for coupled fluid flow, Heat transfer and stress analysis using unstructured moving meshes with cells of arbitrary topology. *Computer Methods in Applied Mechanics and Engineering* 1995; **125**:235–255.
31. Ferziger JH, Peric M. *Computational Methods for Fluid Dynamics*. Springer: Berlin, 1996.
32. Basara B, Jakirlic S, Przulj V. Vortex-shedding flows computed using a new, hybrid turbulence model. Proceedings of *8th International Symposium On Flow Modelling and Turbulence Measurements*, Tokyo, Japan, 4–6 December, 2001.
33. Rhie CM, Chow WL. Numerical study of the turbulent flow past an airfoil with trailing edge separation. *AIAA Journal* 1983; **21**:1525–1532.
34. Van der Vorst. Bi-CGSTAB: a fast and smoothly converging variant of Bi-CG for the solution of nonsymmetric linear system. *SIAM Journal on Scientific Computing* 1992; **13**:631–644.
35. Meijerink JA, Van der Vorst HA. Guidelines for the usage of incomplete decompositions in solving sets of linear equations as they occur in practical problems. *Journal of Computational Physics* 1981; **44**:134–155.
36. Cooper D, Jackson DC, Launder BE, Liao GX. Impinging jet studies for turbulence model assessment. *International Journal of Heat and Mass Transfer* 1993; **36**:2675–2684.
37. Jovic S, Driver D. Reynolds number effects on the skin friction in separated flows behind a backward-facing step. *Experiments in Fluids* 1995; **18**(6):464–467.
38. Hanjalic K, Jakirli S. Contribution towards the second-moment closure modelling of separating turbulent flows. *Computers and Fluids* 1998; **22**(2):137–156.
39. Monson DJ, Seegmiller HL, McConnaughey PK. Comparison of LDV measurements and Navier–Stokes equations in a two-dimensional 180-degree turn-around duct. *AIAA Paper* 89-0275, Reno, Nevada, 1989.
40. Eggels JGM, Boersma BJ, Nieuwstadt FTM. Direct and large-eddy simulations of turbulent flow in an axially rotating pipe. Laboratory for Aero-and Hydrodynamics, Delft University of Technology, Delft, The Netherlands, 1994.
41. Kitoh O. Experimental study of turbulent swirling flow in a straight pipe. *Journal of Fluid Mechanics* 1991; **225**:445–479.
42. Basara B, Alajbegovic A. Steady state calculations of turbulent flows around Morel Body. *Proceedings of the 7th International Symposium On Flow Modelling and Fluid Measurements*, Tainan, Taiwan, 5–8 October, 1998.
43. Lienhart H, Stoots C, Becker S. Flow and Turbulence Structures in the Wake of a Simplified Car Model (Ahmed Model), Wagner *et al*. (eds). *Notes on Numerical Fluid Mechanics*, vol. 77, 2002; 323–330.
44. Patel VC, Rodi W, Scheuerer G. Turbulence models for near-wall and low-Reynolds number flows: a review. *AIAA Journal* 1985; **23**(9):1308–1319.
45. Jones WP, Launder BE. The prediction of the laminarization with a two-equation model of turbulence. *International Journal of Heat and Mass Transfer* 1972; **15**:301–313.

46. Durbin PA. Near-wall turbulence closure modelling without dumping functions. *Theoretical Computer Fluid Dynamics* 1991; **3**:1–13.
47. Kim J, Moin P, Moser R. Turbulence statistics in fully developed channel flow at the low Reynolds number. *Journal of Fluid Mechanics* 1987; **177**:133–166.
48. Kuroda A, Kasagi N, Hirata M. A direct numerical simulation of the fully developed channel flow. *International Symposium on Computational Fluid Dynamics*, Nagoya, 1989; 1174–1179.
49. Laufer J. Investigation of turbulent flow in a two-dimensional channel. *Report NACA TN* 2123, 1950.

